Grain growth, anomalous scaling, and grain boundary grooving in polycrystalline CdTe thin films

Dohyoung Kwon, Yunsic Shim, Jacques G. Amar, and Alvin D. Compaan

Citation: Journal of Applied Physics **116**, 183501 (2014); doi: 10.1063/1.4901068
View online: http://dx.doi.org/10.1063/1.4901068
View Table of Contents: http://scitation.aip.org/content/aip/journal/jap/116/18?ver=pdfcov
Published by the AIP Publishing

Grain growth, anomalous scaling, and grain boundary grooving in polycrystalline CdTe thin films

Dohyoung Kwon, Yunsic Shim, Jacques G. Amar, and Alvin D. Compaan
Department of Physics and Astronomy, University of Toledo, Toledo, Ohio 43606, USA

(Received 13 August 2014; accepted 24 October 2014; published online 10 November 2014)

We examine the evolution of the surface morphology as well as the dynamics of grain growth and grain boundary (GB) grooving in polycrystalline CdTe films sputter deposited on CdS/glass substrates. Anomalous scaling behavior is found with local roughness exponent $\alpha_{loc} = 1$ and global (local) growth exponent $\beta = 0.36$ ($\beta_{\rm loc} = 0.14$). In good agreement with the scaling relation, $\beta_{loc} = \beta - n\alpha_{loc}$, we obtain the correlation length exponent $n = 1/z \simeq 0.23$. We also find that the grain size coarsening exponent p and GB groove growth exponent β_g are both equal to β, while the grain size distribution is well described by a log-normal distribution. These results suggest that GB grooving is responsible for the enhanced anomalous scaling and a deviation from the theoretical prediction of $p = 1/2$, along with the observed log-normal grain size distribution. © *2014 AIP Publishing LLC*. [http://dx.doi.org/10.1063/1.4901068]

I. INTRODUCTION

CdTe-based photovoltaics is one of the fastest growing thin-film solar-cell technologies because of its high absorption coefficient, near optimal bandgap, and low manufacturing cost.[1–6] A variety of deposition techniques as well as post-deposition treatments including annealing and $CdCl_2$ treatments have been used to fabricate high efficiency CdTe solar cells and modules.[6] While the current best efficiency of CdTe solar cells is about 19%,[2] it is still well below the theoretical limit of 29%.[1] The shortfall in the efficiency may be attributed in part to a variety of nano- and micro-scale defects,[7,8] such as point defects[6] (interstitials, vacancies, and antisites), dislocations, twins[9] and grain boundaries[4] formed during the growth of CdTe/CdS films. In addition, the degree of intermixing at the CdTe/CdS interface[3,10,11] and the interface morphology[12,13] also affect the efficiency.

The effects of grain boundaries (GBs) are particularly important since they may significantly reduce the mobility of carriers across the boundaries and also act as sinks for minority carriers.[4] More recently, it has also been shown[14] that in CdTe solar cells doped with Cl, the GBs no longer act as recombination centers but actively contribute to carrier collection. It has also been found that in CdS films the mobility increases with grain size and has a maximum when the grain size is a maximum.[15] These results clearly illustrate the effects of GBs and grain size on the performance of CdTe/CdS thin-film solar cells. However, the surface morphology may also play an important role since it may affect the junction with the following layer. Thus, the surface morphology along with the formation and evolution of GBs[16,17] may have a strong impact on the performance of polycrystalline-based solar cells. We note that progress toward achieving higher efficiency CdTe solar cells has been slowed in part due to the limited understanding of these effects.

Here we present results for the scaling behavior of the surface morphology as well as for the GB evolution in sputter-deposited CdTe thin films grown on sputtered CdS films. We note that recent studies of CdTe films grown via hot-wall epitaxy have examined the surface roughening by using a stylus and found anomalous scaling behavior.[18,19] In addition, the dynamics of grain growth in CdTe films (grown by an electrodeposition technique) after annealing with $CdCl_2$ treatment has also been studied.[20] In contrast, here we examine the dynamics of both surfaces and grain growth as well as grain size distributions during the growth of sputter-deposited CdTe films by using atomic force microscopy (AFM) and scanning electron microscopy (SEM).

Our results indicate that the surface morphology exhibits anomalous scaling behavior with a local roughness exponent $\alpha_{loc} \simeq 1$ and global (local) growth exponent $\beta = 0.36$ ($\beta_{\rm loc} = 0.14$). In good agreement with the scaling relation[21] $\beta_{loc} = \beta - n\alpha_{loc}$, we also find that the exponent n describing the growth of the correlation length ξ with time t (where $\xi \sim t^n$) satisfies $n \simeq 0.23 \pm 0.04$. In addition, both the exponent p describing the growth of the average grain size d_{av} (where $d_{\rm av} \sim t^p$) and the exponent β_g describing the dynamics of GB grooving are equal to β. These results indicate that the evolution of the surface roughness is determined by the dynamics of grain growth and GB grooving.

In addition to these results for the dynamical evolution, we also find that the grain-size distribution is well described by a log-normal distribution. Along with the relatively small value of p ($p < 1/2$) such a distribution is a signature of grain growth stagnation. However, as shown in Sec. III B, the resulting stagnation is not the result of a film thickness effect[22,23] which occurs when the average grain size is comparable to the film thickness. Instead, the formation of GB grooves at the surface and their deepening with time is responsible for the enhanced anomalous scaling behavior and grain growth stagnation. Our AFM and SEM results also indicate that the lateral grain growth is further hampered by the formation of voids between grains.

The organization of this paper is as follows. In Sec. II, we provide the details of experiment for the growth of CdTe/CdS films. In Sec. III, we first present results for the surface

roughening in CdTe films obtained by applying dynamic scaling theory. We then discuss the grain size distributions and the dynamics of grain growth. Finally, in Sec. IV we summarize our results.

II. EXPERIMENT

CdTe/CdS films were deposited by radio-frequency (RF) magnetron sputtering on a Pilkington Tec15 glass coated with a high resistivity transparent (HRT) SnO_2 layer. The glass substrate was thoroughly cleaned with our lab procedure, which has been described elsewhere.[24] Each film was deposited from a 2 in. diameter sputtering target at 10 mTorr of Ar pressure with RF power of 50 W. The deposition rate for CdS was 8.5 nm/min with a resulting thickness of 60 nm, followed by deposition of CdTe at 20.7 ± 0.4 nm/min up to a thickness of 2.5 μm. For the CdTe deposition, only the deposition time was changed, while all other conditions were kept the same. As a result, we found that the thickness of CdTe thin films is linearly proportional to the deposition time. In order to minimize the effects of shadowing and deposition inhomogeneities, during the deposition the substrate was rotated about the substrate normal at a rate of 16.9 rev/min.

The film thickness was measured both with an *in situ* laser interference thickness monitor during deposition using a 980 nm laser diode as well as using a stylus profilometer after deposition. The substrates were heated radiatively by two tungsten lamps in order to maintain a growth temperature of 270 °C. AFM measurements were conducted on a Pico SPM II system (Molecular Imaging) to understand the surface growth in CdTe films. Silicon cantilevers (PPP-NCHR, Nanosensors) of a nominal tip radius of 7 nm were used in tapping mode under ambient conditions with a scan frequency of 2 Hz and resonance frequencies at ~300 kHz. Scan resolution was 1024×1024 pixels with a scan area of $5\ \mu m \times 5\ \mu m$. SEM images were taken with a JEOL JSM-7500F, cold-cathode field-emission microscope. Electron beam acceleration voltage of 2 kV and emission current of 20 μA was typically used. An upper secondary electron image detector was used to capture the image in 30 k magnification.

III. RESULTS

A. Surface roughening in CdTe films

Figure 1 shows AFM images of the initial 60 nm-thick CdS film grown on the HRT-Tec15 substrate along with CdTe films deposited on that CdS film for five different deposition times. Using height profiles obtained from AFM measurements with a lateral pixel size of $L = 1024$, we have examined the surface roughness defined as $w(t) = [\langle h^2(r,t)\rangle - \langle h(t)\rangle^2]^{1/2}$, where $h(r, t)$ is the height of the film at a lateral position r along the substrate and time t while $\langle h(t)\rangle = (1/L^2)\Sigma_r h(r,t)$ is the mean height. The surface roughness of the substrate was initially 17.5 nm, but increased to a value of 23.0 nm after deposition of the 60 nm-thick CdS film. Subsequent deposition of CdTe for 7.5 min on the CdS film (corresponding to a thickness of 155 nm) then resulted in a decrease in the surface roughness by 3 nm, after which there was very little change until a deposition time of 15 min (see Fig. 2(b)) corresponding to a thickness of approximately 300 nm.

The slight decrease in the surface roughness during the first 300 nm of CdTe film growth is likely due to the filling of grooves and/or deep valleys on the surface as a result of the diffusion of Te and Cd. This is supported by recent results obtained from metadynamics[25]-based density functional theory (DFT) calculations[26] at $T = 420$ K in which the free-energy barrier for Te dimer migration on Te-terminated (001) surfaces was found to be small (approximately 0.5 eV). In addition, during this stage of CdTe grain growth, GBs are expected to reorient and migrate in such a way as to reduce the number of high-energy GBs with a high GB groove angle[16] (see inset of Fig. 4(a)). As observed in recent experiments on the annealing of polycrystalline gold films,[27] this tends to reduce the surface roughness. We note that during the early stages of CdTe growth, the effect of interdiffusion

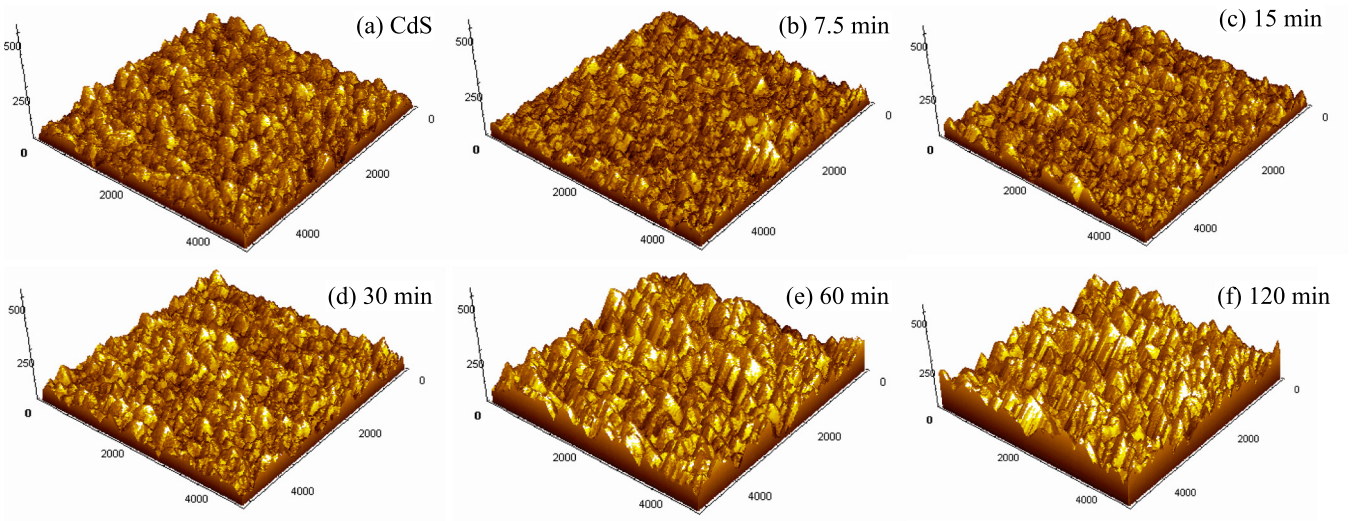

FIG. 1. AFM images of (a) 60 nm-thick CdS films and CdTe films deposited on the CdS films for (b) 7.5 min, (c) 15 min, (d) 30 min, (e) 60 min, and (f) 120 min (2.5 μm).

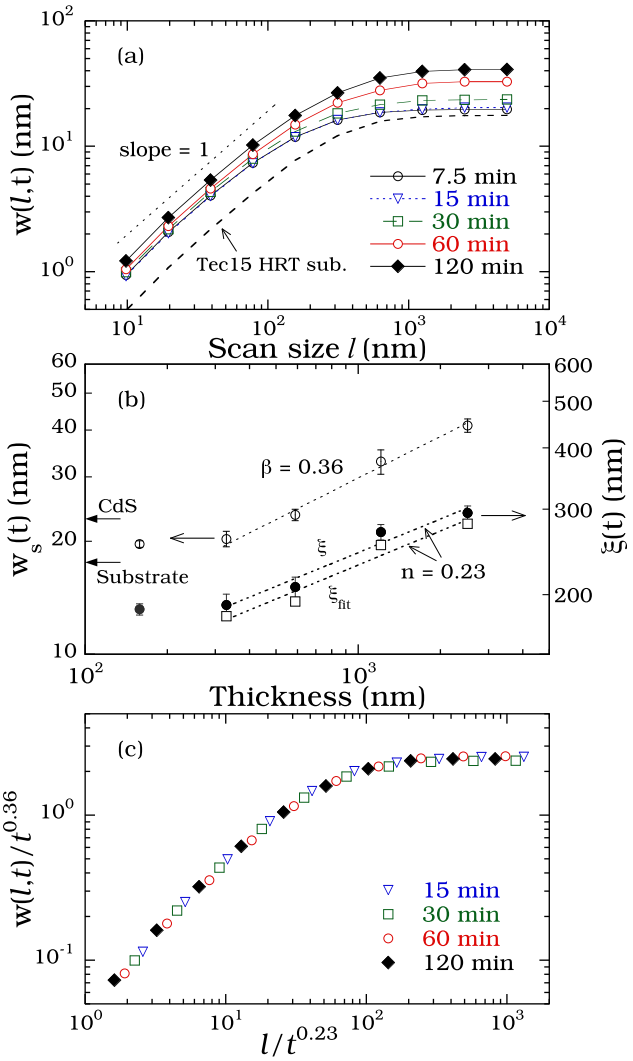

FIG. 2. (a) Surface roughness $w(l, t)$ of CdTe films as function of scan size l at five different deposition times, (b) saturated surface roughness $w_s(t)$ and correlation length $\xi(t)$ and $\xi_{\rm fit}(t)$ obtained from fitting (see text) as function of film thickness t. Dotted lines are power-law fits to data. (c) Scaling of $w(l, t)$ with $\beta = 0.36$ and $n = 0.23$.

at the CdTe/CdS interface on the surface morphology is not likely to be significant since the degree of intermixing between CdTe and CdS at 270 °C ($x = 0.025$) is known to be very small.[28] This is also consistent with experimental results for the activation barrier for bulk diffusion of CdS into CdTe which indicate that it is significantly higher with 2.8 eV.[28]

Further deposition of CdTe then leads to an increase in the surface roughness, as can be seen in Figs. 1(d)–1(f). This increase can be characterized by a power law[29] with the large-scale (saturated) surface roughness increasing as $w_s \sim t^{\beta}$ (see Fig. 2), where t is the film thickness and the growth exponent is estimated as $\beta \simeq 0.36$. In addition, the small-scale surface roughness $w(l)$ measured over an $l \times l$ area increases almost linearly with the scan size l, as shown in Fig. 2(a). Accordingly, we find that the local roughness exponent $\alpha_{\rm loc} = 0.97 \pm 0.05$ (where $w(l) \sim l^{\alpha_{\rm loc}}$). This result is also consistent with the result obtained from the height-height correlation function $G(r,t) = \langle |h(\mathbf{r},t) - h(0,t)|^2 \rangle^{1/2} \sim r^{0.96}$ for $r \ll \xi$.

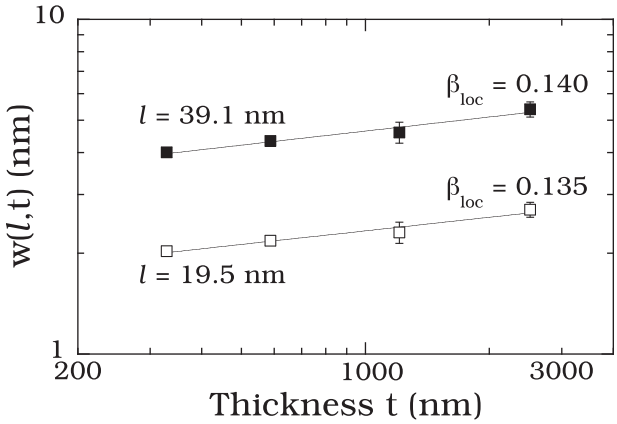

FIG. 3. Surface roughness $w(l, t)$ of CdTe films as function of film thickness t for two different scan sizes.

As shown in Fig. 2(b), the correlation length ξ (defined as the length-scale at which the line joining the first two points in Fig. 2(a) crosses the saturation roughness[30]) satisfies $\xi(t) \sim t^n$ with $n = 0.23 \pm 0.04$, which implies that the dynamic exponent $z = 1/n \simeq 4.3$. A fit to the correlation length $\xi_{\rm fit}(t)$ obtained using the expression, $w(l,t) = w_s(t)[1 - \exp(-(l/\xi_{\rm fit}(t))^{\alpha_{\rm loc}})]$,[31,32] with $\alpha_{\rm loc} = 1$, also yields the same value of the correlation length exponent n. As a result, as shown in Fig. 2(c), the scaling form $w(l, t)/t^{\beta} = f(t/l^n)$ with $\beta = 0.36$ and $n = 0.23$, leads to excellent scaling for $w(l, t)$ as a function of length-scale l and film thickness t.

In general, anomalous scaling is expected to occur[33] when the local roughness exponent $\alpha_{loc} \geq 1$ (see Ref. 34 for a recent review). This is confirmed by the fact that as shown in Fig. 2(a), for small (fixed) l the roughness $w(l, t)$ increases with time, which indicates that the average slope also increases with time. In particular, as shown in Fig. 3, we find $\beta_{\rm loc} \simeq 0.14$ (where $w(l,t) \sim t^{\beta_{loc}}$) which is in good agreement with the scaling relation[21] of $\beta_{\rm loc} = \beta - \alpha_{\rm loc}/z = 0.134$. This result for $\beta_{\rm loc}$ is slightly smaller than the value ($\beta_{\rm loc} \simeq 0.23$) estimated from the case of CdTe growth on TCO-glass substrates by hot-wall epitaxy[18] at 270 °C. The discrepancy may originate from different deposition techniques and growth conditions used in experiments.

We note that in the case of surface growth with relaxation via surface diffusion but no grain-boundary grooving one expects anomalous scaling with $\alpha_{loc} = 1$ and $n = \beta = 1/4$, with an average local slope which grows as $\sqrt{\ln(t)}$ in three dimensions (3D).[33] This anomalous scaling behavior has indeed been observed in Pt growth on glass by sputtering[35] and Si/Si(111) growth by MBE.[36] However, as is found in a variety of other systems,[18,19,37–39] here we find enhanced anomalous scaling with $\beta_{\rm loc} > 0$ rather than logarithmic growth. As indicated by the morphology shown in Fig. 4(a), this enhanced anomalous scaling is most likely due to the effects of GB grooving, which strongly affects GB motion[17] as well as the resulting grain size distribution[23] and also enhances the instability due to surface diffusion.[33]

In the absence of growth, and ignoring the effects of anisotropy, theoretical calculations[16,40] for GB grooving lead to predictions for the increase in the groove height $\Delta H_g(t)$ of

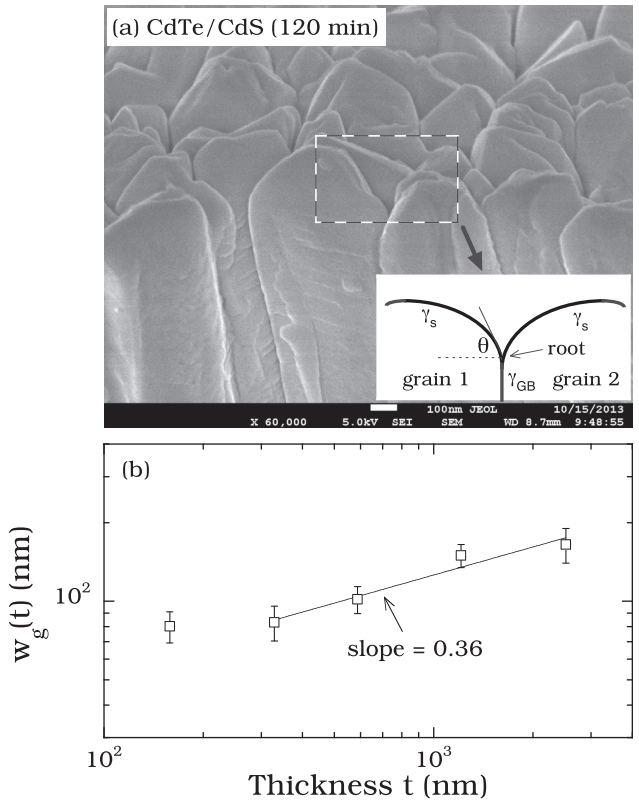

FIG. 4. (a) SEM image of CdTe films at 120 min, where the image was taken with a tilt angle of 60° from the surface normal. Inset shows schematic view of a GB groove for the rectangular region, where θ is the GB groove angle and γ_{GB} and γ_s are the GB free energy and surface free energy per unit area, respectively. In thermal equilibrium, $2\gamma_s sin\theta = \gamma_{GB}$.[16] (b) Width $w_g(t)$ measured from the mean height at the GB groove roots as a function of film thickness t.

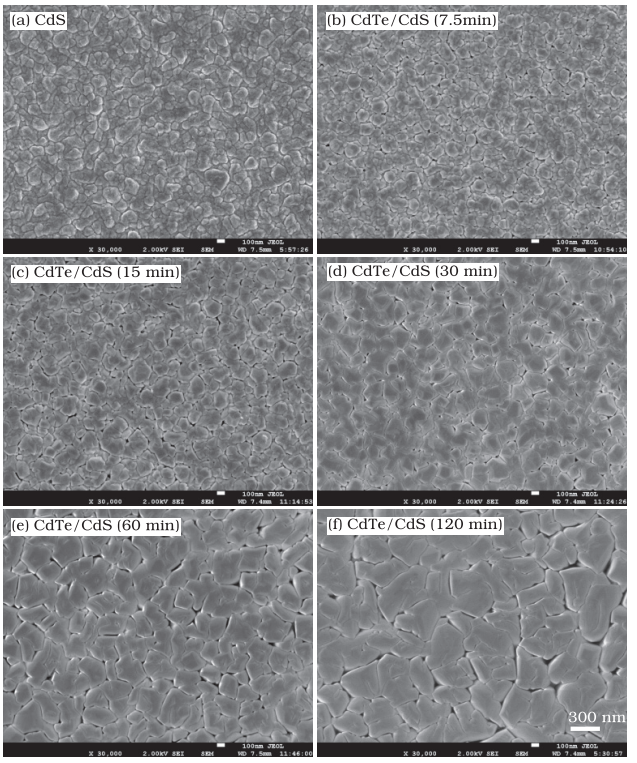

FIG. 5. SEM images of (a) 60 nm-thick CdS films and CdTe films deposited on the CdS films for (b) 7.5 min, (c) 15 min, (d) 30 min, (e) 60 min, and (f) 120 min.

the form $\Delta H_g(t) \sim t^{1/2}$ ($\Delta H_g(t) \sim t^{1/4}$) for the case of surface relaxation dominated via evaporation-condensation (surface diffusion). However, here the effects of growth as well as anisotropy also play an important role. Furthermore, unlike the simple GB groove geometry assumed in these theories, the actual height profiles around GBs are much more complex, as can be seen in Fig. 4(a). As a result, we instead measured the root-mean-square (rms) fluctuation $w_g = \langle (h_g - \langle h \rangle)^2 \rangle^{1/2}$ of the difference between the height h_g of the groove root and the average film height $\langle h \rangle$. As shown in Fig. 4(b), we find that w_g grows with film thickness as $w_g(t) \sim t^{\beta_g}$ with a GB groove growth exponent $\beta_g = 0.36$. The good agreement between the value of this exponent and the surface roughness growth exponent β strongly suggests that the evolution of the surface roughness is determined by the dynamics of GB grooving. However, the fact that the value of β_g found in our experiment differs from the theoretical predictions (1/2 or 1/4) also indicates the complexity of GB grooving processes occurring in growing CdTe polycrystalline films.

B. Grain growth and grain-size distribution in CdTe films

In order to further characterize the CdTe thin-film morphology, we have also studied the evolution of the average grain-size as well as the corresponding grain-size distributions. In particular, as shown by the SEM images in Fig. 5, the average grain size increases with increasing film thickness. The relatively sharp distribution also indicates that there are no abnormally large grains, suggesting that grain growth proceeds in a normal fashion. This also suggests that, as in normal grain growth in the absence of deposition, the main driving force is the lowering of the total free energy of the films by reducing the energy associated with GBs.[41] We note that XRD measurements using $\theta - 2\theta$ geometry for as-deposited CdTe films show a dominant (111) peak, along with very weak peaks at (220) and (311) orientations, while $CdCl_2$ treatments significantly enhance the (220) and (311) peaks.[24]

To further quantify these results, we have measured the distribution of in-plane (lateral) grain sizes, where the in-plane grain size may be defined as $d = \sqrt{4A/\pi}$ and A is the area of grains in the 2D SEM images, separated by GBs and voids. Figure 6 shows the grain size distributions (symbols) for CdS and CdTe films at five different deposition times, where the average grain sizes d_{av} are denoted by arrows. Also shown (solid curves) are fits with a log-normal distribution defined as

$$f(d) = \frac{1}{\sqrt{2\pi}\sigma d} \exp\left[-\frac{(\ln(d) - \mu)^2}{2\sigma^2} \right], \quad (1)$$

where σ is the standard deviation of $\ln(d)$, and μ is the mean of $\ln(d)$.[42] As can be seen, the log-normal distribution fits the data very well. We note that a log-normal distribution has previously been shown to yield a good fit to the experimental

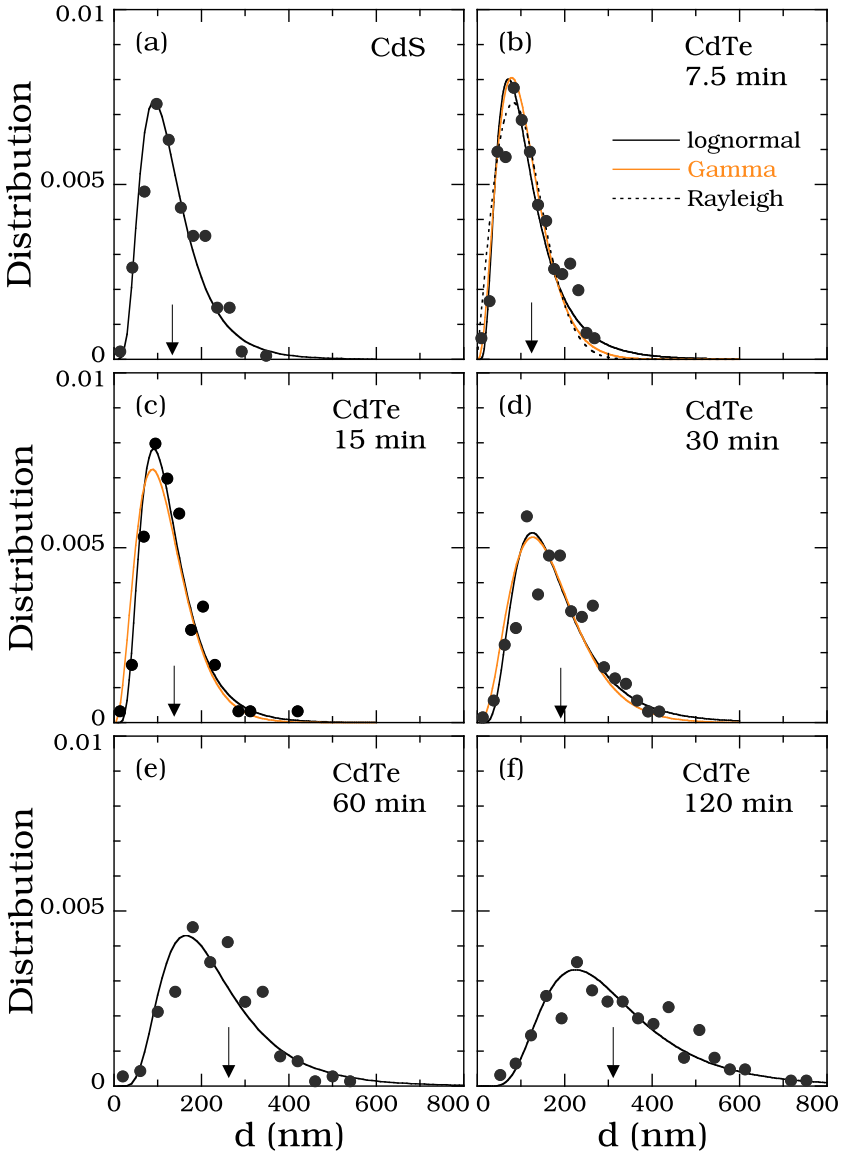

FIG. 6. Grain size distribution for (a) a CdS film on HRT-Tec15 glass substrate and (b)–(f) CdTe films at five different deposition times. Solid lines are log-normal and Gamma fits, while the dotted line is a Rayleigh fit. Average grain sizes d_{av} are denoted by arrows.

grain size distributions observed in a variety of polycrystalline thin films.[22,43–49]

For comparison, we have tested several types of normal grain size distributions including those proposed by Hillert[50] and Louat[51] (Rayleigh distribution[52]) as well as a gamma distribution,[53] and found that the Hillert distribution (not shown) and Rayleigh distribution result in poorer agreement (see Fig. 6(b)). On the other hand, as shown in Fig. 6(b), a gamma distribution (defined as $f_g(x) = x^{\gamma-1}/(b^{\gamma}\Gamma(\gamma))\exp[-x/b]$, where $x = d/d_{av}$) with $\gamma = 3.7$ and $b = 0.25$ also provides a reasonable fit. We note that the gamma distribution has been used to describe Poisson Voronoi cell size distributions in 2D and 3D,[54] which may be relevant for grain nucleation and growth in CdTe films. However, as shown in Fig. 6(c), a gamma function with the same set of parameters appears to deviate from the data for $d/d_{av} < 1$. Moreover, for the grain size distribution shown in Fig. 6(d), the best fit was obtained with $\gamma = 4.0$ and $b = 0.23$. Thus, overall we have found that a log-normal distribution gives a better fit to the grain size distributions observed in CdTe films than a gamma distribution. This is consistent with previous findings for polycrystalline Al films.[44]

Figure 7 shows the average grain size for CdTe films as a function of the film thickness t. Also shown (arrows) are the average grain sizes for the initial HRT-Tec15 substrate as well as for the CdS film just before CdTe deposition. As can be seen, the average grain size increases with a power law, $d_{av}(t) \sim t^{p}$, where the grain growth exponent $p \simeq 0.36 \pm 0.06$. The good agreement between the value of the grain-size coarsening exponent p and the growth exponent β again suggests that the roughness is limited by the grain-size. In addition, we note that a similar value for p ($p \simeq 0.35$) was also obtained previously in CdTe films annealed at 351 °C with $CdCl_2$ treatments.[20] Somewhat similar results, e.g., $p = 0.35$ (0.22) at 160 (280) °C, have also been obtained[55] for polycrystalline Al films.

In contrast to our experimental results, the assumptions of curvature-driven GB motion[50] and random GB motion,[51] lead to the prediction $p = 1/2$ for 3D grain growth. However, the preferred orientation in the case of CdTe growth by sputtering is the (111) orientation[24] which modifies a simple curvature-driven picture of grain growth[41] due to the anisotropy in GB energy and mobility.[56] This is consistent with a

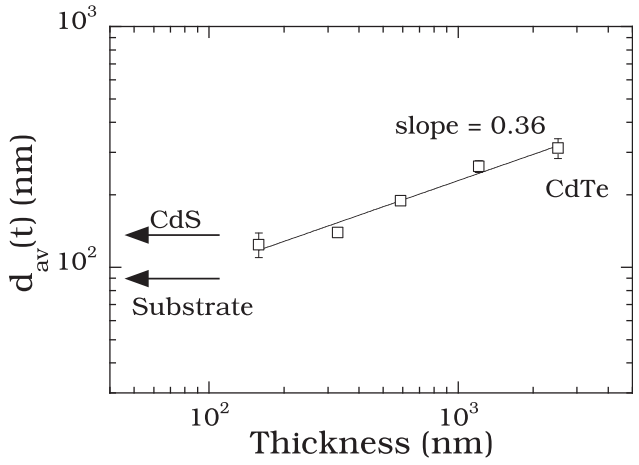

FIG. 7. Average grain size d_{av} (t) as function of film thickness t.

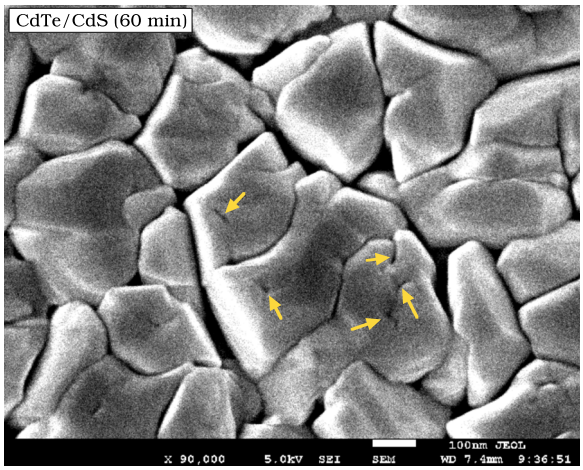

FIG. 8. SEM image of CdTe films at 60 min where the image was taken with a tilt angle of 10° from the surface normal. Yellow arrows indicate defects observed on the surface of grains.

scaling analysis carried out by Thijssen *et al.*,[57] for the 3D Van der Drift model of polycrystalline facet growth, as well as subsequent numerical simulations of this model by Thijssen[58] and Ophus *et al.*[59] which lead to a value ($p = 0.4$) which is in relatively good agreement with our results. As already noted, one possible explanation for the deviation from this value found in our experiments is the presence of grain boundary grooving. In addition, as noted in Ref. 56 other effects such as impurity segregation, and/or second phase particles may also play a role.

In this connection, we note that grain growth during the annealing of thin polycrystalline films may stagnate due to film thickness effects when the average grain diameter d_{av} is two or three times the film thickness t.[22,23] However, this effect may be ignored in this case, since as shown in Fig. 7, the average grain size is significantly smaller than the film thickness at late times. Instead, our anomalous scaling results suggest that GB grooving plays a major role in the stagnation of grain growth in CdTe films. This is consistent with the fact that simulations of grain growth in 2D have also demonstrated that GB grooving leads to a log-normal grain size distribution[23,60] as is observed here.

One possible explanation for the observed anomalous scaling and GB grooving is the presence of various defects and/or imperfections observed on grains, as can be seen in Fig. 8. These defects may act as barriers for diffusing atoms, thus limiting the increase of the correlation length and leading to anomalous scaling. Similarly, we expect that grain growth may also be hampered by the existence of barriers to interfacet and intergrain diffusion. In particular, the existence of barriers to interfacet diffusion may also explain the formation of voids (see Figs. 5(b)–5(d)) which tend to increase in size with increasing film thickness.

IV. SUMMARY

We have examined the surface roughening and grain growth in sputter-deposited polycrystalline CdTe films grown on CdS films/HRT-Tec15 glass substrate. A detailed dynamic scaling analysis of the surface morphology indicates that the CdTe films exhibit anomalous scaling behavior characterized by a non-zero local growth exponent $\beta_{\rm loc} \simeq 0.14$, along with a global growth exponent $\beta = 0.36$, local roughness exponent $\alpha_{\rm loc} \simeq 1$, and correlation length growth exponent $n \simeq 0.23$, which are consistent with the scaling relation $\beta_{loc} = \beta - n\alpha_{loc}$.[21]

While the values of $\alpha_{loc} \simeq 1$ and $n \simeq 1/4$ are consistent with the presence of surface diffusion as the dominant mechanism for surface relaxation over short length-scales, the relatively large value of the global growth exponent is consistent with the observed existence of well-defined facets over larger length-scales, as is assumed in simple models of polycrystalline growth. Thus, both the global growth and GB groove exponents $\beta \simeq \beta_g \simeq 0.36$ are close to the value $\beta = 0.4$ obtained in recent simulations[59,61] of the Van der Drift model of polycrystalline growth in the absence of shadowing. In addition, the relatively large value of the local growth exponent β_{loc} may be explained by the existence of barriers to intragrain, intergrain, and/or interfacet diffusion which lead to GB grooving and hamper the growth of grains.

We have also carried out an analysis of the SEM images of CdTe films on the CdS/HRT-Tec15 which indicates that the grain growth proceeds in a normal fashion (e.g., no abnormally large grains). In particular, a detailed examination of the lateral grain size distributions obtained from the SEM images indicates that a log-normal distribution provides the best description. As discussed above, this is consistent with the existence of GB grooving, which along with the formation of voids between grains tends to hamper the lateral growth. In addition, we find that the grain growth exponent p is equal to the roughness exponent β. This latter result suggests that the limiting factor for the evolution of surface roughness is the grain size, while the limiting factor for grain growth is the diffusion barrier for adatoms to move across grain boundaries.

Finally, we note that while the scaling methods used here have provided significant insight into the mechanisms of surface roughening, relaxation, and grain boundary evolution during the growth of sputter-deposited CdTe thin-films, these methods have also widely been used to study the

dynamics of a variety of other nonequilibrium systems. In particular, it would be interesting to apply these methods in order to understand the key mechanisms which affect the growth of other photovoltaic thin-films, such as $Cu(In,Ga)Se_2$ (CIGS) and other chalcogenide materials. In this connection, we are currently extending the present study to a variety of growth substrates, growth parameters and post-growth treatments to determine the best pathway to improved solar-cell performance characteristics.

ACKNOWLEDGMENTS

D. Kwon gratefully acknowledges support from NSF grant CHE-0840474 and the assistance of Dr. Pannee Burckel for SEM use at the Instrumentation Center at the University of Toledo. Y. Shim and J. G. Amar also acknowledge support from NSF Grant DMR-0907399.

[1]T. M. Razykov, C. S. Ferekides, D. Morel, E. Stefanakos, H. S. Ullal, and H. M. Upadhyaya, Sol. Energy **85**, 1580 (2011).
[2]M. A. Green, K. Emery, Y. Hishikawa, W. Warta, and E. D. Dunlop, Prog. Photovolt.: Res. Appl. **21**, 827 (2013).
[3]K. D. Dobson, I. Visoly-Fisher, G. Hodes, and D. Cahen, Sol. Energ. Mater. Sol. Cells **62**, 295 (2000).
[4]A. L. Fahrenbruch, J. Cryst. Growth **39**, 73 (1977).
[5]K. Durose, P. R. Edwards, and D. P. Halliday, J. Cryst. Growth **197**, 733 (1999).
[6]B. E. McCandless and J. R. Sites, *Handbook of Photovoltaic Science and Engineering*, 2nd ed., edited by A. Luque and S. Hegedus (Wiley and Sons, UK, 2011).
[7]J. Versluys, P. Clauws, P. Nollet, S. Degrave, and M. Burgelman, Thin Solid Films **451-452**, 434 (2004).
[8]D. K. Ward, X. W. Zhou, B. M. Wong, F. P. Doty, and J. A. Zimmerman, Phys. Rev. B **85**, 115206 (2012).
[9]Y. Yan, M. M. Al-Jassim, and K. M. Jones, J. Appl. Phys. **94**, 2976 (2003).
[10]M. D. G. Potter, M. Cousins, K. Durose, and D. P. Halliday, J. Mater. Sci.: Mater. Electron. **11**, 525 (2000).
[11]Y. L. Soo, S. Huang, Y. H. Kao, and A. D. Compaan, Appl. Phys. Lett. **74**, 218 (1999).
[12]S. Huang, Y. L. Soo, Y. H. Kao, and A. D. Compaan, J. Vac. Sci. Technol. A **19**, 2181 (2001).
[13]Y. L. Soo, S. Huang, Y. H. Kao, and A. D. Compaan, J. Appl. Phys. **83**, 4173 (1998).
[14]C. Li, Y. Wu, J. Poplawsky, T. J. Pennycook, N. Paudel, W. Yin, S. J. Haigh, M. P. Oxley, A. R. Lupini, M. Al-Jassim, S. J. Pennycook, and Y. Yan, Phys. Rev. Lett. **112**, 156103 (2014).
[15]L. L. Kazmerski, W. B. Berry, and C. W. Allen, J. Appl. Phys. **43**, 3515 (1972).
[16]W. W. Mullins, J. Appl. Phys. **28**, 333 (1957).
[17]W. W. Mullins, Acta Metall. **6**, 414 (1958).
[18]A. S. Mata, S. C. Ferreira, I. R. B. Ribeiro, and S. O. Ferreira, Phys. Rev. B **78**, 115305 (2008).
[19]F. S. Nascimento, S. C. Ferreira, and S. O. Ferreira, EPL **94**, 68002 (2011).
[20]B. Qi, D. Kim, D. L. Williamson, and J. U. Trefmy, J. Electrochem. Soc. **143**, 517 (1996).
[21]J. M. López, Phys. Rev. Lett. **83**, 4594 (1999).
[22]J. E. Palmer, C. V. Thompson, and H. I. Smith, J. Appl. Phys. **62**, 2492 (1987).
[23]H. J. Frost, C. V. Thompson, and D. T. Walton, Acta Metall. Mater. **38**, 1455 (1990).
[24]D. Kwon, Ph.D. Dissertation (University of Toledo, 2012).
[25]A. Laio and F. L. Gervasdio, Proc. Natl. Acad. Sci. USA **99**, 12562 (2002).
[26]F. Pietrucci, G. Gerra, and W. Andreoni, Appl. Phys. Lett. **97**, 141914 (2010).
[27]M. J. Rost, D. A. Quist, and J. W. M. Frenken, Phys. Rev. Lett. **91**, 026101 (2003).
[28]B. E. McCandless, M. G. Engelmann, and R. W. Birkmire, J. Appl. Phys. **89**, 988 (2001).
[29]F. Family and T. Vicsek, J. Phys. A **18**, L75 (1985).
[30]A.-L. Barabasi and H. E. Stanley, *Fractal Concepts in Surface Growth* (Cambridge University Press, Cambridge, 1995) and references therein.
[31]S. K. Sinha, E. B. Sirola, S. Garoff, and H. B. Stanley, Phys. Rev. B **38**, 2297 (1988).
[32]H.-Y. Yang, T.-M. Lu, and G.-C. Wang, Phys. Rev. B **47**, 3911 (1993).
[33]J. G. Amar, P.-M. Lam, and F. Family, Phys. Rev. E **47**, 3242 (1993).
[34]L. Guo, G. Oskam, A. Radisic, P. M. Hoffmann, and P. C. Searson, J. Phys. D: Appl. Phys. **44**, 443001 (2011).
[35]J. H. Jeffries, J.-K. Zuo, and M. M. Craig, Phys. Rev. Lett. **76**, 4931 (1996).
[36]H.-N. Yang, G.-C. Wang, and T.-M. Lu, Phys. Rev. Lett. **73**, 2348 (1994).
[37]S. Huo and W. Schwarzacher, Phys. Rev. Lett. **86**, 256 (2001).
[38]B. C. Mohanty, H.-R. Choi, and Y. S. Cho, J. Appl. Phys. **106**, 054908 (2009).
[39]I. Lee and E. Park, J. Phys. Soc. Jpn. **80**, 124602 (2011).
[40]H. A. Stone, M. J. Aziz, and D. Margetis, J. Appl. Phys. **97**, 113535 (2005).
[41]C. V. Thompson, Annu. Rev. Mater. Sci. **30**, 159 (2000).
[42]S. K. Kurtz and F. M. A. Carpay, J. Appl. Phys. **51**, 5725 (1980).
[43]M. Vopsaroiu, G. V. Fernandez, M. J. Thwaites, J. Anguita, P. J. Grundy, and K. O.'Grady, J. Phys. D: Appl. Phys. **38**, 490 (2005).
[44]D. T. Carpenter, J. R. Codner, K. Barmak, and J. M. Rickman, Mater. Lett. **41**, 296 (1999).
[45]M. Huang, Y. Wang, and Y. A. Chang, Thin Solid Films **449**, 113 (2004).
[46]N. Tigau, V. Ciupina, G. Prodan, G. I. Rusu, and E. Vasile, J. Cryst. Growth **269**, 392 (2004).
[47]K. O'Grady, L. E. Fernandez-Outon, and G. Vallejo-Fernandez, J. Magn. Magn. Mater. **322**, 883 (2010).
[48]K. Barmak, E. Eggeling, D. Kinderlehrer, R. Sharp, S. Taasan, A. D. Rollett, and K. R. Coffey, Prog. Mater. Sci. **58**, 987 (2013).
[49]R. Backofen, K. Barmak, K. E. Elder, and A. Voigt, Acta Mater. **64**, 72 (2014).
[50]M. Hillert, Acta Metall. **13**, 227 (1965).
[51]N. P. Louat, Acta Metall. **22**, 721 (1974).
[52]C. S. Pande and K. P. Cooper, Acta Mater. **59**, 955 (2011).
[53]M. F. Vaz and M. A. Fortes, Scr. Metall. **22**, 35 (1988).
[54]K. Marthinsen, Mater. Charact. **36**, 53 (1996).
[55]C. Eisenmenger-Sittner, J. Appl. Phys. **89**, 6085 (2001).
[56]M. P. Anderson, D. J. Srolovitz, G. S. Grest, and P. S. Sahni, Acta Metall. **32**, 783 (1984).
[57]J. M. Thijssen, H. J. F. Knops, and A. J. Dammers, Phys. Rev. B **45**, 8650 (1992).
[58]J. M. Thijssen, Phys. Rev. B **51**, 1985 (1995).
[59]C. Ophus, E. J. Luber, and D. Mitlin, Phys. Rev. E **81**, 011601 (2010).
[60]C. Lou and M. A. Player, J. Phys. D: Appl. Phys. **35**, 1805 (2002).
[61]C. Ophus, T. Ewalds, E. J. Luber, and D. Mitlin, Acta Mater. **58**, 5150 (2010).